JOURNAL OF COMPUTATIONAL PHYSICS 71, 324–342 (1987)

Numerical Investigation of the Disintegration of Liquid Jets

F. SHOKOOHI

Breed Corporation, Boonton Township, New Jersey 07005

AND

H. G. ELROD

Professor of Engineering Science, Columbia University, New York, New York 10028

Received November 25, 1985; revised September 5, 1986

A numerical investigation of the capillary instability and disintegration of infinite liquid jets of a circular cross section is carried out All the nonlinear and viscous terms are included. A vorticity-stream function formulation is used in conjunction with a new computer-generated numerical algorithm to ensure the requisite accuracy and to facilitate the treatment of the free surface boundary. Successive surface profiles are compute. These results show that the nonlinear terms are responsible for the nonuniformity of the sizes of drops produced in jet disintegration In the case of a jet of water, satellites are obtained for all the unstable disturbances treated. The sizes of these satellites are found to increase with the disturbance wavelength. The computed drop sizes for a jet of water are generally in good agreement with the experimental observations of previous investigators.

1. INTRODUCTION

The problem of disintegration of jets was first investigated experimentally by Savart [1] in 1833. Subsequent to Savart's work, Plateau [2], calculating the potential energy of the disturbed configuration, showed that a cylindrical column of inviscid liquid in vacuua is stable for all purely nonaxisymmetric disturbances, but is stable or unstable for axisymmetric disturbances according to whether their wavelengths are less or greater than the circumference of the undisturbed column.

Rayleigh [3] included the kinetic energy of the associated motion of the disturbed configuration and arrived at an equation for the growth rate of a symmetrical disturbance. Specifically, he found that a disturbance having a wavelength 4.51 times the diameter of the jet grows more rapidly than any other, and eventually breaks up the jet into droplets.

In a second analysis, Rayleigh [4] included the effects of viscosity. This analysis resulted in a complicated dispersion relation which was not conducive to solution. Assuming the viscous effects to be very large compared with inertia effects, he

0021-9991/87 $3.00

showed that the maximum instability occurs when the wavelength of the disturbance is very large compared with the diameter of the undisturbed jet, i.e., when the wavelength is theoretically infinite.

It was Bassett [5], and later Weber [6], who obtained a quantitative description of the instability of a viscous jet. They found that viscosity does not alter the stability criterion predicted by Plateau, but that viscous effects increase the wavelength of the most rapidly growing disturbance.

Since the hydrodynamical equations are nonlinear, a linear theory can be expected to break down. In the first place, it conserves mass only to first order. Second, a linear theory does not exlain the nonsinusoidal surface shapes observed in experiment. Furthermore, the experimental studies of Donally and Glaberson [7] show that large main drops are interspaced with smaller drops (satellites) which are not accounted for by the linear theory. These observations mean that a higher order theory is imperative to a better understanding of the disintegration pheonmenon.

Yuen [8], using the method of strained coordinates, developed a third-order theory and calculated the higher order terms of the surface deformation. Thus, for an inviscid jet, he shows the nonsinusoidal development of an initially sinusoidal wave. His analysis also shows that for short wavelengths the rate at which the neck contracts is greater than the rate at which the swell grows, whereas for long wavelengths, the contrary is true. However, he found that the maximum growth rate occurs at the wavelength given by Rayleigh's linear theory. Other theoretical investigations on the nonlinear instability of inviscid jets were performed by Nayfeh [9] and Wang [10], and more recently by Lafrance [11]. Lafrance's approach closely resembles that of Yuen. His nonlinear analysis predicts the appearance of satellites, and his results are in good agreement with the experimental data of Rutland and Jameson [12].

Yuen also performed experiments which strongly supported his own theory. According to both Lafrance's analysis and experiments, satellites cease at dimensionless wavenumbers less than 0.8. However, Rutland and Jameson observed that satellites are always formed, albeit they are very small at large wavenumbers. The experiments of Goedde and Yuen [13] confirm this latter viewpoint.

Even though the problem of disintegration of liquid jets has been subjected to many analytical treatments, there has still been a need for a comprehensive study of the phenomenon. Theories to date have either dealt with a linearized form of the problem, or have been based on the assumption of an inviscid jet. In this paper, we present a numerical solution to the problem, including both nonlinear and viscous terms. Our numerical approach, in addition to being of a more general nature, provides more flexibility in dealing with the problem. Here a vorticity stream function formulation is employed to solve the Navier–Stokes equations numerically. A newly developed algorithm is used to provide accuracy and to falitate treatment of the free-surface boundaries. Sizes of main and satellite drops are computed over a range of disturbance wavelengths.

2. The Jet Model and Governing Equations

We consider a jet emerging from a nozzle of radius, a (see the Appendix). Immediately after emergence, stress relaxation occurs at the outer surface, and the velocity profile tends to uniformity. If the maximum rate of growth of any disturbance is such that the jet can travel a substantial number of diameters downstream before any breakup occurs, then the jet can be treated as uniform and infinite for the purpose of a stability analysis. All of the cited prior analyses involve the assumption that these conditions are satisfied, and the assumption is retained here as well. In addition, friction with the jet surroundings is neglected, on the presumption that the surrounding medium is a low-density, low-viscosity gas. Only axisymmetric disturbances are treated, principally for expediency, but justified partially by some theoretical argument that these disturbances are the most unstable [2]. Cylindrical coordinates are used for our analysis, with "z" along the jet axis.

The radial and axial components of the equation of motion for an incompressible fluid of viscosity with axisymmetric motion about axis z are

$$\frac{Du}{Dt} = -\frac{1}{\rho}\frac{\partial p}{\partial r} + \nu\left(\frac{\partial^2 u}{\partial r^2} + \frac{1}{r}\frac{\partial u}{\partial r} - \frac{u}{r} + \frac{\partial^2 u}{\partial z^2}\right) \tag{1}$$

where

$$\frac{Dw}{Dt} = -\frac{1}{\rho}\frac{\partial p}{\partial z} + \nu\left(\frac{\partial^2 w}{\partial r^2} + \frac{1}{r}\frac{\partial w}{\partial r} + \frac{\partial^2 w}{\partial z^2}\right) \tag{2}$$

$$\frac{D}{Dt} = \frac{\partial}{\partial t} + u\frac{\partial}{\partial r} + w\frac{\partial}{\partial z} \tag{3}$$

and u and w are the radial and axial components of velocity, respectively, p is the pressure, and $\nu = \mu/\rho$ is the kinematic viscosity.

The equation of mass continuity is

$$\frac{\partial u}{\partial r} + \frac{u}{r} + \frac{\partial w}{\partial z} = 0 \tag{4}$$

which is satisfied by letting

$$u = \frac{1}{r}\frac{\partial \psi}{\partial z}; \qquad w = -\frac{1}{r}\frac{\partial \psi}{\partial r}, \tag{5}$$

ψ, being the Stokes' stream function.

Eliminating p between Eqs. (1) and (2), one obtains the so-called "vorticity transport equation":

$$\frac{D\omega}{Dt} - \frac{u\omega}{r} = \nu\nabla^2\omega - \frac{\nu\omega}{r^2}, \tag{6}$$

where ω is the component of vorticity normal to the r–z plane and is given by

$$\omega = \frac{\partial u}{\partial z} - \frac{\partial w}{\partial r}. \tag{7}$$

Furthermore, ω is related to ψ by the following relation

$$r\omega = D\psi, \tag{8}$$

where the differential operator D is defined as

$$D \equiv \frac{\partial^2}{\partial r^2} - \frac{1}{r}\frac{\partial}{\partial r} + \frac{\partial^2}{\partial z^2}. \tag{9}$$

3. Boundary Conditions

3.1. *Surface Conditions*

In order to simplify the formulation of the surface conditions, a coordinate system locally tangent to the free surface is chosen (Fig. 1). The surface conditions may be expressed as follows:

(a) Vanishing of the shear stress at the surface yields:

$$\left(\frac{\partial u}{\partial r} - \frac{\partial w}{\partial z}\right)\sin(2\alpha) + \left(\frac{\partial u}{\partial z} + \frac{w}{r}\right)\cos(2\alpha) = 0. \tag{10}$$

(b) The difference in the normal stress between the inside and outside of the jet is due to the interfacial surface tension. This condition is formulated as

$$p - p_a = 2\mu\left(\frac{\partial u}{\partial r}\cos^2\alpha + \frac{\partial w}{\partial z}\sin^2\alpha\right) - \mu\left(\frac{\partial u}{\partial z} + \frac{\partial w}{\partial r}\right)\sin(2\alpha) + \sigma\left\{r_s^{-1}\left[1 + \left(\frac{\partial r_s}{\partial z}\right)^2\right]^{-1/2} - \frac{\partial^2 r_s}{\partial z^2}\left[1 + \left(\frac{\partial r_s}{\partial z}\right)^2\right]^{-3/2}\right\}, \tag{11}$$

where p_a is the ambient pressure and r_s is the disturbed radius of the jet.

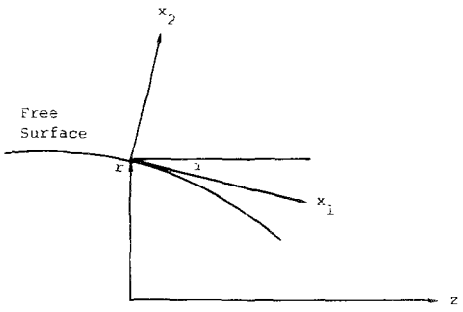

FIGURE 1

(c) Every point on the surface of the jet must always adhere to the surface and not flow through it. This kinematical condition can be mathematically expressed as

$$\frac{\partial r_s}{\partial t} = u_s - w_s \frac{\partial r_s}{\partial z} \tag{12}$$

where u_s and w_s are the radial and axial velocities, respectively, at the surface of the jet.

3.2. *Centerline Conditions*

At the centerline of the jet, one may specify

$$\psi = 0 \qquad \text{at} \quad r = 0. \tag{13}$$

For the axial velocity to be finite at $r = 0$, the following restriction must hold

$$\frac{\partial \psi}{\partial r} = 0 \qquad \text{at} \quad r = 0. \tag{14}$$

Furthermore, because of symmetry of the axial velocity with respect to the centerline, Eq. (7) yields

$$\omega = 0 \qquad \text{at} \quad r = 0. \tag{15}$$

4. Numerical Solution Procedure

4.1. *Transformation of Coordinates*

We replace the variable "r" by η as independent variable. Thus:

$$\eta = r/r_s(z, t) \tag{16}$$

During the process of computation, this transformation enables one to accomplish:

(a) Retention of an adequate number of grid points as the jet contracts.

(b) Maintenance of high precision on the boundary by having a point exactly on the surface.

(c) Uniformity of grid size in the transformed coordinates (η, z).

However, these desirable characteristics are achieved at the expense of complicating the differential equations, and proliferating the derivative terms in the boundary conditions.

4.2. *Order of Calculations*

Suppose that at time t all the physical variables of the flow are known. Then the kinematic condition (12) is used to determine the new shape of the jet. Using new

values of r_s and current values of u and w, one solves Eq. (6) with appropriate boundary conditions to compute the vorticity in the jet interior. Next, using the new values of r_s and current values of u and w, one solves Eq. (7) with pertinent boundary conditions for ψ. Finally, u and w everywhere, and ω at the surface are computed. The computation cycle is repeated.

4.3. *Numerical Solution of the Vorticity Transport Equation*

The numerical solution of the vorticity transport equation is obtained by the application of the well-known alternating-direction implicit method (ADI). This method was developed by Peaceman and Rachford (14) and by Douglas (15) for multidimensional heat flow and diffusion. In a Cartesian coordinate system, for one half time step, it treats values of the dependent variable along successive lines of constant x_i as unknowns, with all other values known. Thus along any given x_i, the unknowns form a tridiagonal matrix which is readily solved. During the following half time step, a similar procedure is used in the y direction. So used, the method is unconditionally stable, with a truncation error of

$$O(\Delta t) + O((\Delta \eta)^2) + O((\Delta z)^2).$$

The remapping of coordinates used in the present paper causes cross derivatives to appear in the differential equation. It will be observed that the *ADI method always evaluates such cross-derivative finite-difference terms explicitly*. Some degradation in the timewise truncation error can be expected.

4.4. *Numerical Solution of ψ–ω Relation*

In order to obtain an accurate numerical solution to Eq. (8), a newly developed algorithm is used. This algorithm consists of a constraint between functional values at the nine pivotal points of the grid shown in Fig. 2. To obtain this algorithm, ψ is expanded into a polynomial of 17 terms about the grid center as

$$\begin{aligned}\psi = {} & a_{00} + a_{10}\eta + a_{20}\eta^2 + a_{30}\eta^3 + a_{40}\eta^4 + a_{01}z + a_{02}z^2 \\ & + a_{03}z^3 + a_{04}z^4 + a_{11}\eta z + a_{12}\eta z^2 + a_{21}\eta^2 z + a_{22}\eta^2 z^2 \\ & + a_{14}\eta z^4 + a_{41}\eta^4 z + a_{31}(\eta^3 z + \eta z^3) + a_{42}(\eta^4 z^2 + \eta^2 z^4)\end{aligned} \tag{17}$$

where η and z here are measured from the grid center. Evaluation of this polynomial at each of the 9 points gives rise to 9 linear equations. Further, sub-

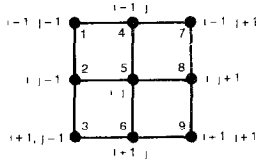

FIGURE 2

stitution of this polynomial into the ψ–ω relation (8) with subsequent satisfaction at the 9 points produces 9 more equations. Thus one arrives at a system of 18 linear equations in 17 unknowns a_{ij}. For compatibility, there must be a constraint between values of ψ and ω at the pivotal points of the grid. This relation can be written as

$$\sum_{i=1}^{q} \beta_i \psi_i = \sum_{i=1}^{q} \beta_{i+q} \Omega_i, \tag{18}$$

where "i" designates the grid point, β_i are the metric coefficients, and

$$\Omega \equiv r\omega.$$

Obtaining similar relations for other grids, one arrives at the following system of linear equations

$$[B]\{\psi\} = \{G\}. \tag{19}$$

The elements of the two-dimensional matrix B and the vector G consist of the respective values of β and $\beta\Omega$ throughout the computation field.

Although highly accurate, the foregoing numerical technique is relatively uneconomical in time and so is used in regions where accuracy is more difficult to achieve, that is, along lines $i=2$ (see next section), $i=3$, and along line $i=N-1$ (see Section 4.6) (Fig. 3).

In order to save computation time, an alternative high-accuracy scheme, as shown in Fig. 4, was used elsewhere in the computation field. Let $L_{25}(\psi)$ denote the 5×5 difference operator corresponding to the differential operator in Eq. (8). Let $L_9(\psi)$ denote the same for a 3×3 central difference scheme. Then one may write:

$$L_q(\psi) - L_{25}(\psi) + L_{25}(\psi) = Q. \tag{20}$$

The difference $L_{25} - L_9$ is small, and can be treated explicitly. Thus

$$L_{25}(\psi) = Q - [L_q(\psi) - L_{25}(\psi)]. \tag{21}$$

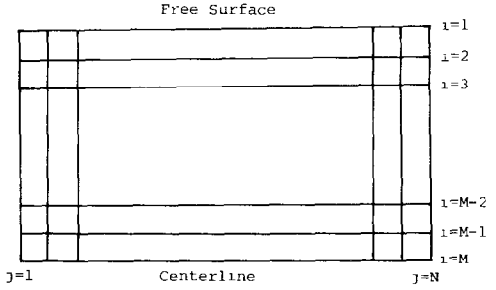

FIGURE 3

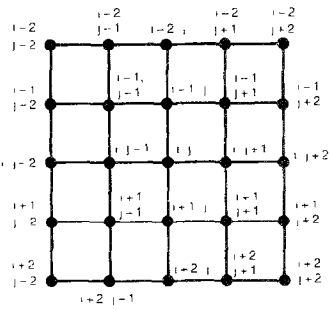

FIGURE 4

This argument gives essentially the higher order accuracy with the lower-order formula.

The system of linear equations thus obtained is linked to the system (19) and the resulting total system is subsequently solved by ADI. As previously noted. ADI evaluates all cross derivatives explicitly.

4.4. *Numerical Treatment of the Surface Conditions*

Equations (10) and (11) constitute the boundary conditions at the surface of the jet. Upon eliminating p from Eqs. (2) and (11), one arrives at a rather complicated equation which, in conjunction with Eq. (10) (expressed in (η, z) coordinates), is used as the surface condition throughout the computation. Transient terms introduced in Eq. (11) as a result of the elimination of p are treated implicitly.

Let us again consider the 9-point grid shown in Fig. 2. In order to obtain the algorithm corresponding to surface conditions (11) and (12), we use the following procedure. The polynomial (17) is substituted into the surface conditions, which are imposed at points 1, 4, and 7, thus producing six equations. Twelve other equations are obtained in the manner descrived in Section (4.3). Thus one arrives at the surface algorithm, which is a constraint between the ψ's and ω's at points 2, 3, 5, 6, 8, and 9.

4.5. *The Centerline Algorithm*

The streamfunction at the centerline is subjected to the conditions

$$\psi = 0 \qquad \text{and} \qquad \frac{\partial \psi}{\partial r} = 0 \qquad \text{at } r = 0.$$

Furthermore, the algorithm must be such that it can withstand the variation of $1/r$ in Eq. (8). In our experience, the polynomial (17) tolerated this variation near the centerline very well, and an algorithm was obtained in the same manner as in Section 4.3, except that at points 3, 6, and 9 (which are located on the centerline), the conditions imposed are $\psi = 0$ and $\partial \psi / \partial \eta = 0$.

4.6. *Surface Velocity, Surface Vorticity, and Contour Calculations*

At every point along the line $i=2$ of Fig. 3, ψ is expanded into a polynomial about the center of the grid. This polynomial is represented by (17) and can be written in matrix notation as

$$\psi_k = \{a\}\{F\}_k, \tag{22}$$

where $\{a\}$ and $\{F\}_k$ are 17-component vectors, one consisting of the unknown coefficients and the other of the known terms of the polynomial. The subscripts $k=1, 2,..., 9$ designate the positions on the grid.

The simultaneous evaluation of the polynomial, Eq. (8) and the surface conditions at the nine grid points, results in a set of 18 linear equations in 17 unknowns. This system can be represented by

$$[c]\{a\} = \{b\}, \tag{23}$$

where $[c]$ is an 18×17 coefficient matrix and $\{b\}$ is an 18×1 column matrix constituting 18 known quantities. Elimination of any of these equations, say the 14th, from this system enables one to solve for $\{a\}$. Once $\{a\}$ is computed, any derivative of ψ can be expressed as

$$D_{ij}\psi]_k = \{a\}\{D_{ij}F\}_k, \tag{24}$$

where i and j denote the order of the differentiation with respect to η and z, respectively. For example,

$$D_{10}\psi]_5 = \{a\}\{D_{10}F\}_5$$

means

$$\frac{\partial\psi}{\partial\eta}\Big]_5 = \{a\}\left\{\frac{\partial F}{\partial\eta}\right\}_5,$$

where the subscript 5 corresponds to the position on the grid.

The velocity components along the surface and along the line $i=2$ are computed using the aforementioned procedure. However, in the interior, the velocity components are obtained using the usual three-point central difference formula. Near the centerline, where $\eta \to 0$ (Fig. 5), these formulas are not applicable. The con-

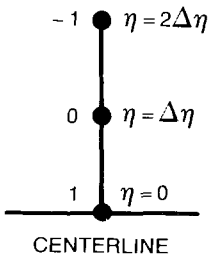

FIGURE 5

dition $\partial\psi/\partial\eta = 0$ at the centerline must be realized by any formulation that yields the velocity distribution in that vicinity. Furthermore, the radial symmetry of w must be incorporated. These considerations call for the expansion formula for ψ near the centerline,

$$\psi = A\eta^2 + B\eta^4$$

where

$$A = \frac{16\psi_0 - \psi_{-1}}{12(\Delta\eta)^2}$$

and

$$B = \frac{\psi_{-1} - 4\psi_0}{12(\Delta\eta)^4}.$$

The value of the vorticity at the surface is also obtained by computing the coefficients of the polynomial (17) and substituting the polynomial into Eq. (8).

The new contour of the jet is determined by the kinematic condition (12), which can be written as

$$\frac{\partial}{\partial t}(r_s)^2 = 2\{a\}\{D_{01}F\}_4.$$

An explicit treatment of the time derivative gives

$$(r_s)^{n+1} = (r_s)^n + 2(\Delta t)\{a\}\{D_{01}F\}_4, \tag{25}$$

where n is the time index.

4.7. *Numerical Differentiation of r_s*

It can be seen that the spatial derivatives of r_s occur frequently in the coefficients of the governing equations and surface conditions. In order to obtain these quantities, one has to differentiate numerically the updated values of r_s computed via Eq. (25). Cubic splines, which exclude none of the data, are used for this purpose. This procedure generates a function which is continuous, together with its first two derivatives, at every point. Spline functions are discussed in Ref. (16).

4.8. *Inflow–Outflow Conditions*

It is easy to show that the nonlinear governing equations must preserve the nodal symmetry of any disturbance which is initially sinusoidal. Thus in the numerical calculations the wavelength of the disturbance is held constant by prescribing periodicity at the right and left ends of the computation field. In other words, the wavelength of an initial disturbance is kept fixed throughout the computation, as one observes the growth or oscillation, as the case may be, of that particular disturbance. For the infinitely long jet, this treatment substitutes for inflow–outflow conditions.

4.9. *Initial Conditions*

The jet is assumed to be moving with a uniform over its cross section and to be displaced from equilibrium by an infinitesimal disturbance. The perturbation quantities are taken to be those of Rayleigh's linearized solution for an inviscid jet at $t=0$. The new geometry of the jet is determined with the use of the value of r_s from Rayleigh's solution at $t=\Delta t$. All flow configurations thereafter are computed numerically.

5. Results

5.1. *Drop Sizes*

Figures 6 through 13 demonstrate the effects of the wavelength of an axially symmetric disturbance upon the stability of a jet of water. Figures 6 and 7 show that disturbances having wavelengths less than D are stable and propagate as waves. Furthermore, as one might expect, the propagation speed decreases with increasing wavelength, and disturbances having shorter wavelengths dampen faster than those with longer wavelengths. At the cutoff wavelength for small-disturbance inviscid theory, $\lambda=\pi D$, Fig. 8 shows that disturbances experience some growth. Nevertheless, the growth rate is small, and this fact is demonstrated in Fig. 9, where the contour is plotted at $T=20$. The Basset–Weber theory predicts that viscosity does not affect the stability criterion of Plateau. Thus one may conclude that the

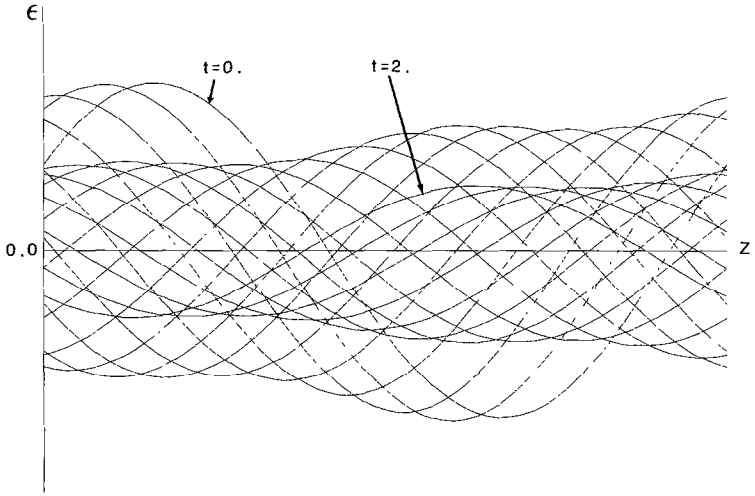

Fig. 6. Propagation of a disturbance of stable mode: infinite jet nonlinear solution. diameter of the undisturbed jet $D=0.0035$ cm, wavelength of the disturbance = 1.00 D, initial amplitude of the disturbance = 0.01 D, viscosity of the liquid = 0.01 g/(cm*s), surface tension of the liquid = 72.5 erg/cm^2, density of the liquid = 1.00 g/(cm**3), $T=2.00$.

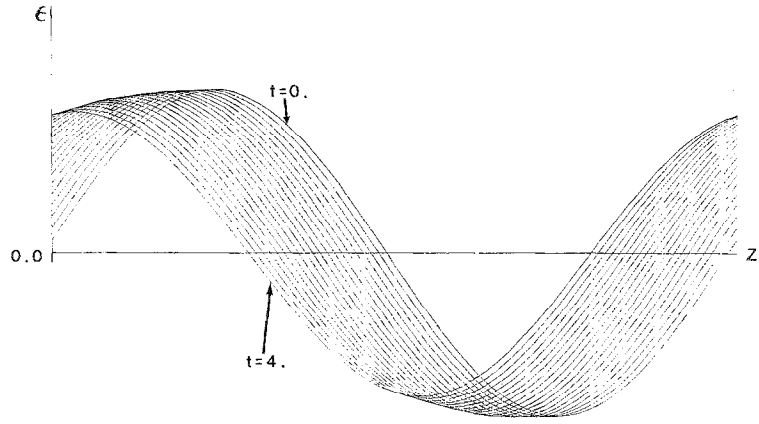

FIG. 7. Proagation of a disturbance of stable mode: infinite jet nonlinear solution: diameter of the undisturbed jet D = 0.0035 cm, wavelength of the disturbance = 2.80 D, initial amplitude of the disturbance = 0.01 D, viscosity of the liquid = 0.01 g/(cm*s), surface tension of the liquid = 72.5 erg/cm^2, density of the liquid = 1.00 g/(cm**3), $T = 4.00$.

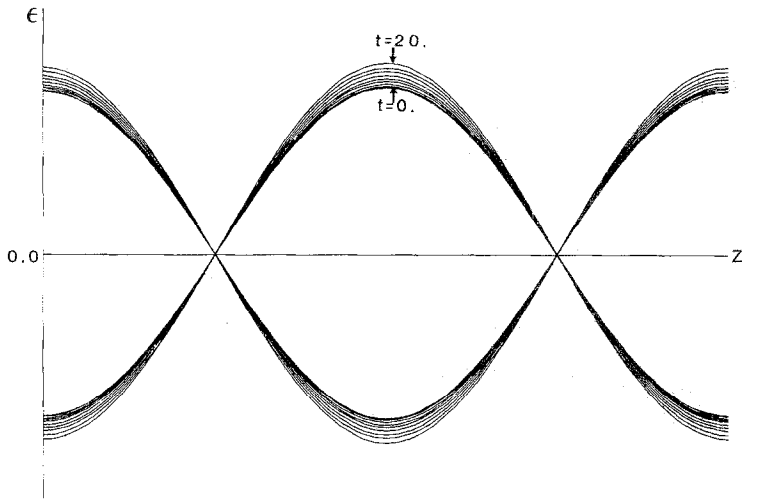

FIG. 8. Growth of a disturbance having the invisced theory's cutoff wavelength: infinite jet nonlinear solution: diameter of the undisturbed jet D = 0.0035 cm, wavelength of the disturbance = 3.14 D, initial amplitude of the disturbance = 0.01 D, viscosity of the liquid = 0.01 g/(cm*s), surface tension of the liquid = 72.5 erg/cm^2, density of the liquid = 1.00 g/(cm**3), $T = 20.00$.

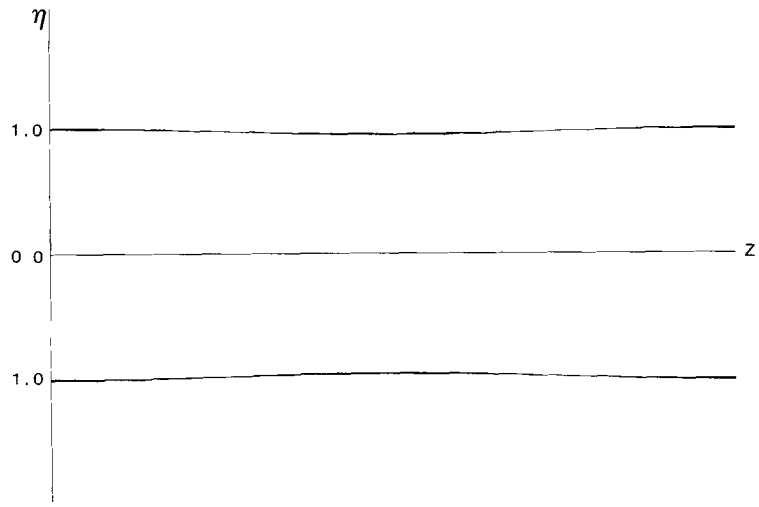

FIG. 9. Jet profile for a disturbance having the inviscid theory's cutoff wavelength: infinite jet nonlinear solution: diameter of the undisturbed jet D = 0.0035 cm, wavelength of the disturbance = 3.14 D, initial amplitude of the disturbance = 0.01 D, viscosity of the liquid = 0.01 g/(cm*s), surface tension of the liquid = 72.5 erg/cm^2, density of the liquid = 1.00 g/(cm**3), T = 20.00.

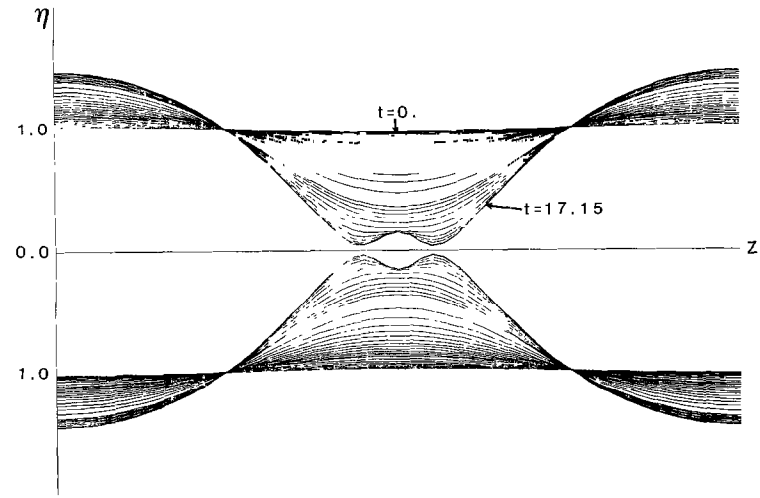

FIG. 10. Infinite jet nonlinear solution: diameter of the undisturbed jet D = 0.0035 cm, wavelength of the disturbance = 3.30 D, initial amplitude of the disturbance = 0.01 D, viscosity of the liquid = 0.01 g/(cm*s), surface tension of the liquid = 72.5 erg/cm^2, density of the liquid = 1.00 g/(cm**3), T = 17.15.

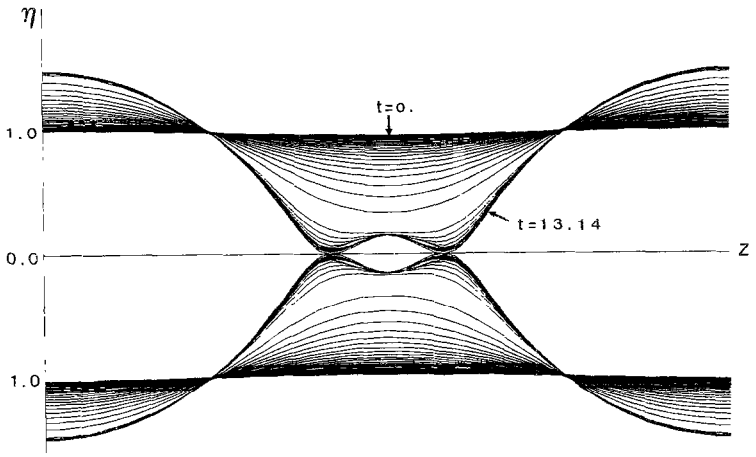

FIG. 11 Infinite jet nonlinear solution: diameter of the undisturbed jet $D = 0.0035$ cm, wavelength of the disturbance = 3 500 D, initial amplitude of the disturbance = 0.01 D, viscosity of the liquid = 0.01 g/(cm*s), surface tension of the liquid = 72.5 erg/cm^2, density of the liquid = 1.00 g/(cm**3), $T = 13.14$.

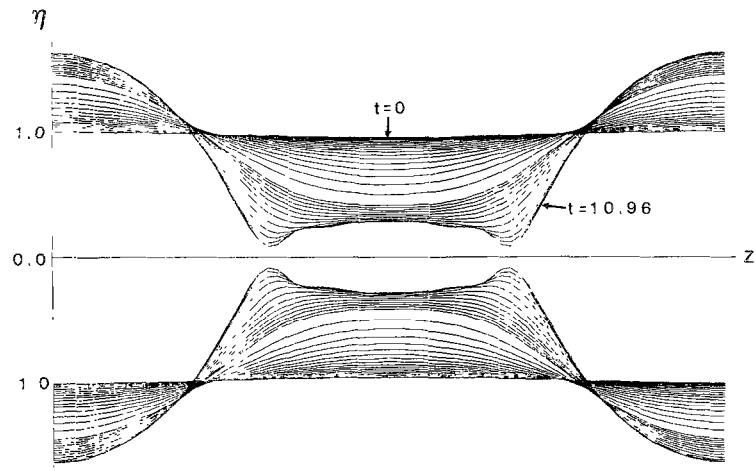

FIG. 12. Infinite jet nonlinear solution: diameter of the undisturbed jet D = 0.0035 cm, wavelength of the disturbance = 4.508 D, initial amplitude of the disturbance = 0.01 D, viscosity of the liquid = 0.01 g/(cm*s), surface tension of the liquid = 72.5 erg/cm, density of the liquid = 1.00 g/(cm**3), $T = 10.96$

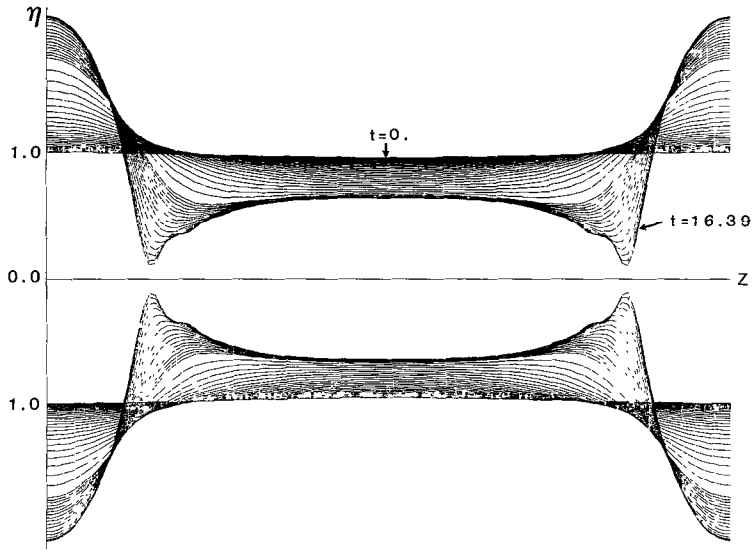

FIG. 13. Infinite jet nonlinear solution: diameter of the undisturbed jet D = 0.0035 cm, wavelength of the disturbance = 9.00 D, initial amplitude of the disturbance = 0.01 D, viscosity of the liquid = 0.01 g/(cm*s), surface tension of the liquid = 72.5 erg/cm^2, density of the liquid = 1.00 g/(cm**3), $T = 16.39$.

decrease in the threshold of stability is a nonlinear effect, as asserted by Yuen and Nayfeh. Figures 10 through 13 show the instability, and eventual breakup, of a jet of water into main and satellite drops when the initial disturbance has a wavelength greater than πD. One may observe that, for shorter wavelengths, the neck contracts faster than the swell grows. For longer wavelengths, the contrary becomes true. According to Rayleigh's inviscid linear theory and Yuen's nonlinear inviscid analysis, a disturbance having a wavelength of 4.5080 grows fastest. Our numerical results show that, due to viscous effects, the wavelength of the fastest growing disturbance should be just slightly larger than this value.

Drop radii are plotted in Fig. 14. These computed results show that the size of the satellites increases with the wavelength of the initial disturbance. Drop radii were calculated from drop volumes at incipient breakup. A comparison between theory and previous experimental measurements is presented in Fig. 15. According to Lafrance's theory, satellites cease to be present for nondimensional wavenumbers greater than 0.8 ($\lambda < 3.93D$). However, our computed results predict satellites in that range.

5.2. *Tests for Accuracy*

As is customary in such numerical work, it is necessary to demonstrate that the results obtained are insensitive to increment size. In Ref. [17], it is shown that, typically, a twofold variation in Δz and a tenfold variation in Δt make no

significant difference. However, to preserve such insensitivity to the time increment near jet breakup, it was necessary to reduce further the increment magnitude. A typical value for Δz was about 0.4 and, for Δt, about 0.1.

The adequacy of the choice of $\Delta\eta = 0.1$, which was used uniformly in all calculations, is justified by the results in Fig. 16. Here the transient velocities resulting from sudden stress relaxation at the surface of a Poiseuille flow are compared with the exact series solution obtained from Ref. [18]. This is a severe test, and the agreement is excellent.

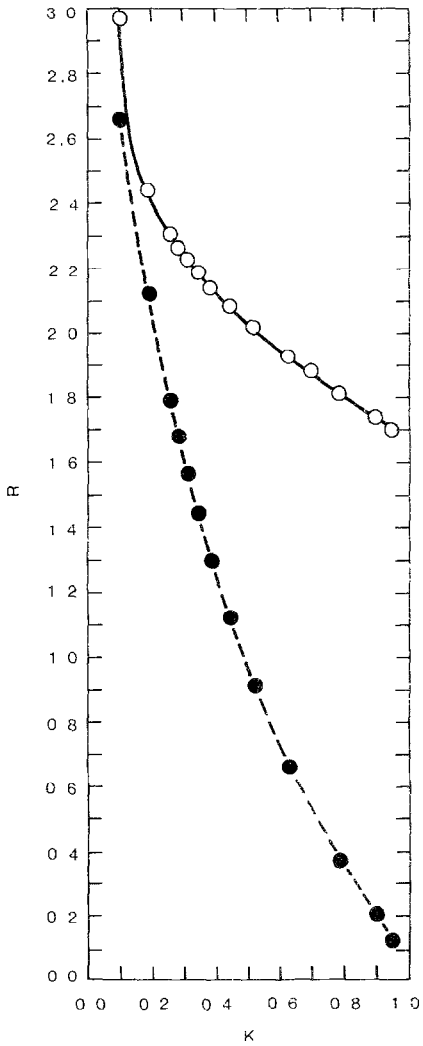

FIG 14. Drop radius variation with wavenumber for the breakup of a jet of water as predicted by the present numerical solution: ○, main drop; ●, satellite drop.

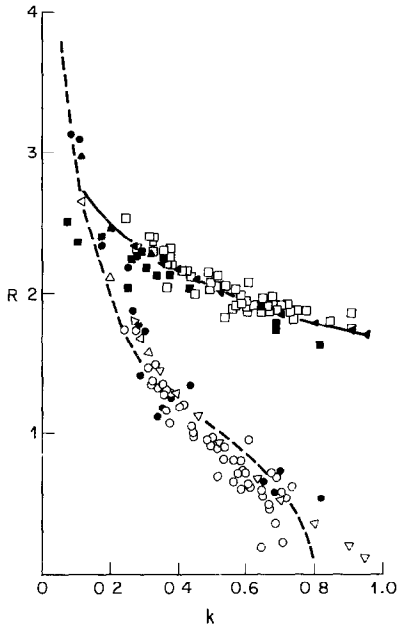

FIG. 15. Comparison of the drop sizes obtained from the present numerical solution for a jet of water with the previous theoretical predictions and experimental measurements. Theory: Lafrance, ———, main drop; – – –, satellite drop; numerical, ▲, main drop; ⎵, satellite drop. Experiment: Rutland and Jameson, ■, main drop; ●, satellite drop; Lafrance, □, main drop; ○, satellite drop.

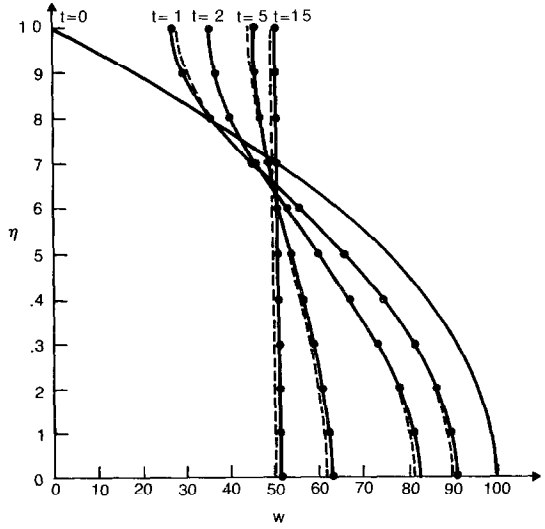

FIG. 16 Comparison of the axial elocity profile of an infinite jet with zero initial disturbance against the temperature profile in an infinite pipe with zero heat flux at the wall. The initial velocity and temperature distributions are given by $100(1-\eta^2)$. Diameter of the undisturbed jet = D = 0.0035 cm; viscosity of the liquid = 0.01 g/(cm*s); surface tension of the liquid = 1.00 erg/cm^2; density of the liquid = 1.00 g/(cm**3).

Both accuracy and numerical stability were established by additional tests. Zero-viscosity numerical results agree in the linear range very well with Rayleigh's solution for both stable and unstable modes, and for the threshold wavelength. In Figs. 8 and 9, there is no evidence of numerical instability for computations involving 200 time steps on a slightly disturbed viscous jet with a disturbance wavelength at the inviscid linear threshold. Indeed, for all computations performed with the chosen increments of η, z, and t, there were no indications of numerical instability.

APPENDIX: NOMENCLATURE

a	Undisturbed jet radius
D	Undisturbed jet diameter
i	Index in r direction
j	Index in z direction
k	Dimensionless wavenumber
M	Number of divisions in r direction
n	Iteration index, time index
N	Number of subdivisions in z direction
p	Pressure
p_a	Ambient pressure
r	Radial position
r_s	Jet radius
R	Dimensionless drop radius
R_1, R_2	Mutually orthogonal principal radii of curvature
t	Time
T	Total time
u	Radial component of velocity
w	Axial component of velocity
z	Axial position coordinate
α	Angle between local tangent to jet surface and the z axis
Δr	Increment in r direction
Δz	Increment in z direction
ξ	Surface deformation $= r_{z=a}$
η	r/r_s
λ	Wavelength of disturbance
μ	Viscosity
ν	Kinematic viscosity
ρ	Density
σ	Surface tension
ψ	Stokes' stream function
ω	Component of vorticity normal to r–z plane
Ω	$r\omega$

ACKNOWLEDGMENTS

F. Shokoohi was the recipient of an IBM fellowship, which is here gratefully acknowledged. Dr. Richard Toupin of IBM Research, Yorktown, suggested the study and provided continuous encouragement and advice.

REFERENCES

1. F. SAVART, *Ann. Chim. (Paris)* **53**, 337 (1833).
2. J. PLATEAU, *Statique Experimentale et Théorique des Liquids Soumis aux Seules Forces Moleculaires* (Gauthier–Villars, Paris, 1873).
3. LORD RAYLEIGH, *Proc. London Math. Soc.* **10**, 4 (1978).
4. LORD RAYLEIGH, *Philos. Mag.* **34**, 145 (1894).
5. A. B. BASSET, *Amer. J. Math.* **16**, 13 (1894).
6. C. WEBER, *Z. Angew. Math. Mech.* **2**, 136 (1931).
7. R. J DONALLY AND W GLABERSSON, *Proc. Roy. Soc. London A* **290**, 547 (1966).
8. M. C YUEN, *J. Fluid Mech.* **33**, 151 (1968).
9. A. H. NAYFEH, *Phys. Fluids* **13**, 841 (1970).
10. D. P. WANG, *J. Fluid Mech.* **34**, 299 (1968).
11. P. LAFRANCE, *Phys. Fluids* **18**, 428 (1975).
12. D. P. RUTLAND AND G. J. JAMESON, *J. Chem. Eng. Sci.* **25**, 1689 (1970).
13. E. F. GOEDDE AND M. C. YUEN, *J. Fluid Mech.* **40**, 495 (1970)
14. D. W. PEACEMAN AND H. H. RACHFORD, JR., *J. Soc. Ind. Appl. Math.* **3**, 28 (1955).
15. J DOUGLAS, *J. Soc. Ind. Appl. Math.* **3**, 42 (1955).
16. J. H. AHLBERG, E. N. NILSON, AND J. L. WALSH, *The Theory of Splines and Their Applications* (Academic Press, New York, 1967).
17. F. SHOKOOHI, Ph.D. thesis, Columbia University, 1976 (unpublished).
18. H. S. CARSLAW AND J. C. JAEGER, *Conduction of Heat in Solids.* (Oxford Univ. Press (Clarendon), London/New York, 1959).